AIAA 81-0377R

Remote Measurements of Trace Species in the Troposphere

R. L. Byer* and M. Endemann†
Stanford University, Stanford, Calif.

A reliable single ended remote monitoring laser infrared radar (lidar) operating in the infrared is described. The system uses a 1.4-4.0 μm tunable optical parametric oscillator (OPO) source as transmitter. Continuous remote monitoring of atmospheric methane over a 17-h period demonstrates the reliability of the system. Simultaneous remote measurements of temperature and humidity using absorption lines of the 1.9-μm water band achieve relative accuracies of 1.0°C and 1%, respectively, over a 45 s averaging period. The expected sensitivity for the measurement of other pollutants with absorption lines within the tuning range of the transmitter is discussed.

I. Introduction

THE need for single-ended air pollution monitoring systems is now well established and the methodology of making remote measurements is understood.[1] The monitoring of industrial pollution and the measurement of trace constituents are done efficiently using a single-ended remote probing technique. Furthermore, remote probing is evolving into an important research tool for studying transport, mixing, and chemistry of trace constituents in the atmosphere. Recent experiments have also shown the potential for simultaneous remote humidity and temperature measurements for meteorology.

In their review article Kildal and Byer[2] found that remote measurements using absorption promised the highest sensitivity and lowest required power levels. In a later paper, Byer and Garbuny[3] analyzed remote measurement methods including single-ended absorption with topographic targets and depth resolved absorption using Mie scattering as a distributed retroreflector. For long path absorption a narrow bandwidth laser beam is transmitted through the atmosphere to a distant topographic target. Some portion ρ of this beam is scattered back by the noncooperative target, and is collected by a telescope at the transmitter end. The received energy $S(\nu)$ is determined by using conservation of energy leading to the laser infrared radar (lidar) equation

$$S(\nu)=E_0(\nu)\frac{\eta A}{R^2}\rho^*\exp\left[-2\int_0^R\{\alpha_{sca}(r)+N(r)\sigma(\nu)\}dr\right] \quad (1)$$

where

E_0 = transmitted light-energy of frequency ν
η = efficiency of optical system
A = area of receiving telescope
R = distance to backscattering target
$\rho(R)$ = backscattering due to target at distance R
α_{sca} = attenuation coefficient due to atmospheric scattering losses
$N(r)$ = number density of species to be probed
$\sigma(\nu)$ = absorption cross section of species at wavelength ν

In the near infrared, topographic targets scatter 1-10% of the incident light back toward the receiving telescope. The average concentration of a pollutant along the lightpath $N\equiv\int N(r)dr/R$ is measured by transmitting two pulses with different frequencies ν. If the frequency change is small, only the absorption cross section of the pollutant changes, so that the concentration N derived from Eq. (1) is

$$N=\frac{\ell n\{S(\nu_1)/S(\nu_2)\}}{2R\{\sigma(\nu_2)-\sigma(\nu_1)\}} \quad (2)$$

where the absorption cross sections $\sigma(\nu_i)$ have been determined previously. Fixed frequency lasers have only a few coincidences with absorption lines of interest[4] so that for most applications a tunable laser is preferred.

From 1974 on many remote monitoring systems have been developed and tested using tunable dye lasers.[5,6] Initially the reliability of many of these systems was marginal, but recently a number of systems with excellent reliability using commercially available Nd:Yag pumped dye lasers have been reported.[7,8] A series of field measurements have demonstrated the usefulness of remote pollution detection.[8] However, dye laser measurements in the visible and ultraviolet region are limited to the measurement of only three pollutants: SO_2, NO_2, and O_3.

To extend the lidar measurements to other atmospheric constituents, the infrared spectral region must be used. Line tunable CO_2, and recently doubled CO_2 and DF lasers have been used,[9-11] but are limited to spectral coincidences with absorption lines of pollutant molecules. To achieve wider pollutant selection and better measurement sensitivity, we have developed a continuously tunable high-power infrared source which is used as transmitter for a single-ended remote measurement system. The transmitter is an optical parametric oscillator (OPO), which is continuously tunable from 1.4 to 4.0 μm. Initial measurements of SO_2 (Ref. 12) and also CH_4 (Ref. 13) with this system have been reported by Baumgartner and Byer. Improvements in the design of the OPO transmitter which increased the reliability and spectral resolution considerably were described by Brosnan and Byer.[14] Increased output energy up to 70 mJ per pulse at 10 Hz was achieved with an optical parametric amplifier (OPA) discussed by Baumgartner and Byer.[15] Extensive software development has enabled automatic pollution measurements to be made over timescales of many hours as demonstrated by recent CH_4 measurements.[16]

II. System Description

The Stanford lidar transmitter is an angle phasematched, singly resonant $LiNbO_3$ optical parametric oscillator. For the methane measurements the OPO was amplified by an optical parametric amplifier. OPO and OPA are described in detail by Brosnan and Byer[14] and Baumgartner and Byer.[15]

Presented as Paper 81-0377 at the AIAA 19th Aerospace Sciences Meeting, St. Louis, Mo., Jan. 12-15, 1981; submitted March 6, 1981; revision received July 30, 1981.

*Professor of Applied Physics, Applied Physics Department, Edward L. Ginzton Laboratory of Physics.
†Research Scientist, Battelle Institute e.v., Frankfurt, W. Germany.

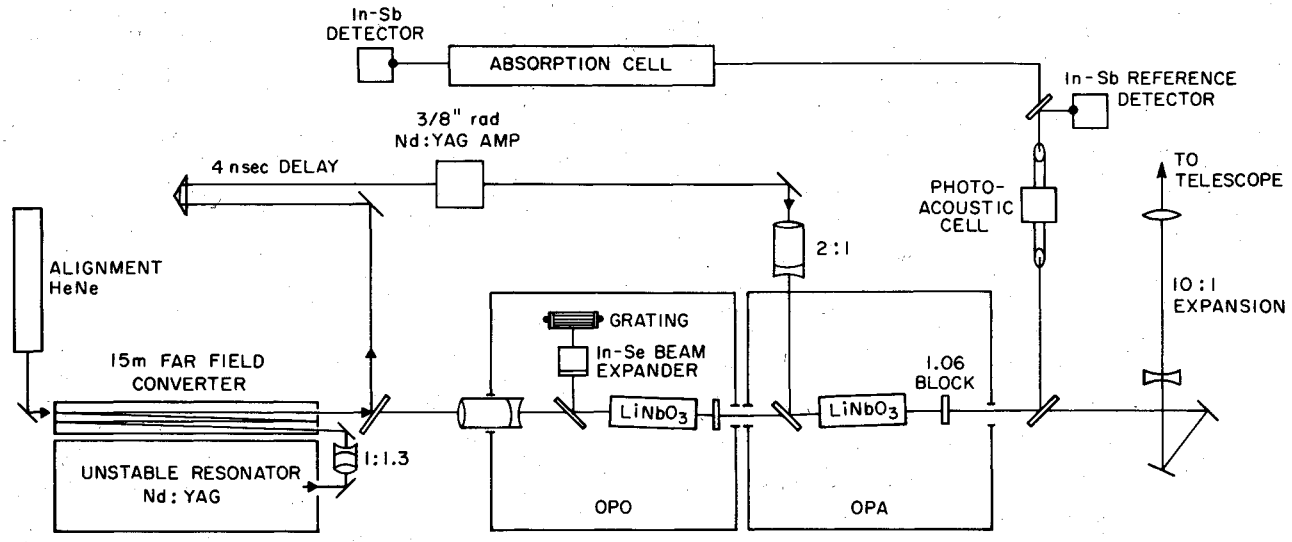

Fig. 1 Schematic of the 1.4-4.0-μm tunable transmitter.

Table 1 Parameters of the OPO-lidar

	CH_4 measurement	Temperature measurement
Transmitter	OPO/OPA	OPO
Frequency range	2917-2922 cm^{-1}	5650-5652 cm^{-1}
Energy/pulse	7 mJ	5 mJ
Pulse length	10 ns	10 ns
Pulse repetition rate	10 Hz	10 Hz
Linewidth (FWHM)	1.4 cm^{-1}	0.1 cm^{-1}
Receiver		
Light collector	Newtonian telescope	Newtonian telescope
Diameter	400 mm	400 mm
Focal length	1.2 m	1.2 m
Detector	InSb at 77 K	InSb at 77 K
Detector D^*	$1.3 \cdot 10^{11}$ (cm$\sqrt{\text{Hz}}$/W)	$4 \cdot 10^{10}$ (cm$\sqrt{\text{Hz}}$/W)
Electronics		
Impulse response time	300 ns	300 ns

Figure 1 shows a diagram of the transmitter. The Q-switched unstable resonator Nd:Yag laser generates 220 mJ energy per pulse with a 10 Hz repetition rate. The length of the resonator is 1.40 m to generate 18-ns long Q-switched pulses. This pulse length is ideal to pump the OPO, since the optical intensity of the pump beam is low enough to avoid damage of the $LiNbO_3$ crystal due to self focusing, but the oscillation threshold of the OPO still is low due to decreasing buildup losses.[14]

The output of the Nd:Yag laser is slightly demagnified to a 5-mm-diam beam and directed into a folded 15-m long path. This distance is adequate to transform the unstable resonator 1.06-μm beam into the far field Airy-disk mode with 60% of the beam energy in the central lobe. Oscillation threshold of the OPO is decreased considerably with this pump beam compared to pumping with the near field unstable mode. The danger of surface damage to the $LiNbO_3$ crystal is also removed. The pointing stability of the long-cavity Nd:Yag laser and the far-field converter is critical for the reliability of the system. We used fused silica rods to stabilize the Nd:Yag resonator structure, and mounted the steering mirrors for the folded 15-m path length far-field converter directly onto the laser resonator structure. This arrangement gives excellent pointing stability of the beam.

For operation of the OPA 40% of the 130 mJ of 1.06-μm energy is split off into a Nd:Yag amplifier, while the main part is directed through a 2.2$\times$demagnifying telescope to pump the OPO. The OPO uses a 50-mm long, 20-mm-diam $LiNbO_3$ crystal to generate the signal and idler output. The signal wave tunes from 2.1 to 1.4 μm, while the idler wave tunes from 2.1 to 4.0 μm for a 4 deg change in the $LiNbO_3$ phase matching angle. The tuning range is limited by absorption of the idler wave in the $LiNbO_3$ crystal at 4 μm. The OPO uses an L-shaped resonator which reflects only the signal wave. The resonator uses a flat output coupler with 50% reflectivity between 1.4 and 2.1 μm, and a 600 grate/mm grating. In order to improve the resolution of the grating, a 10:1 ZnSe prism beam expander[17] is inserted into the cavity. With grating and prism beam expander the linewidth at half intensity points is less than 0.8 cm^{-1} for the signal wave. To improve the resolution further, a tilted etalon can be inserted into the cavity. For a 2-mm thick etalon the signal output linewidth is less than 0.1 cm^{-1}. The linewidth of the idler output is about equal to the sum of the widths of signal and pump beam. The Nd:Yag laser has a linewidth of 0.4 cm^{-1}, but can be reduced easily to 0.01 cm^{-1} by inserting a tilted etalon.

Output energy of the OPO is 5 mJ in the signal wave over most of the tuning range. Due to the absorption losses of the idler wave in the $LiNbO_3$ crystal, the threshold increases near the end of the tuning range and the output energy decreases. The energy of the idler output is equal to the energy in the signal wave multiplied by the ratio of the photon energies.

Astigmatic beam divergence was observed in the OPO output beams when the grating-prism beam expander is used for linewidth control. With the etalon the output beam has a symmetrical divergence and can be collimated.

The OPA consists of a Nd:Yag pumped 50$\times$20-mm angle phasematched $LiNbO_3$ crystal. It increases the output energy from the OPO to more than 12 mJ in the signal wave.

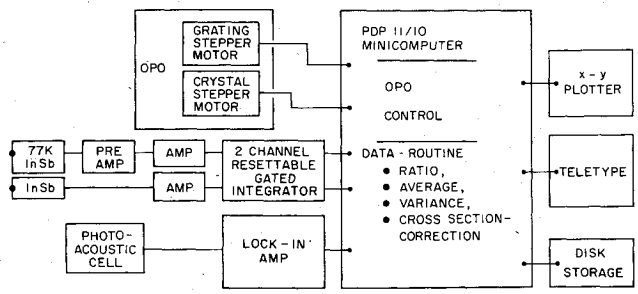

Fig. 2 Schematic of the electronics and data processing based on PDP-11/10 minicomputer.

However, for the temperature and humidity measurements only the OPO was used. This simplified the setup, and yet provided enough energy to see a strong backscattering signal from topographic targets. Table 1 summarizes the transmitter parameters for the different measurements.

About 1% of the tunable light energy is used for diagnostic purposes. The lack of wavelength resettability of the OPO in early experiments led to the introduction of a photoacoustic cell to monitor the proper tuning of the OPO by observing the absorption cross section during an extended measurement. Improvements of the tuning mechanism made continuous monitoring of the cross section superfluous and later the cell was used only for spectroscopic measurements. An InSb detector is used as reference detector to ratio out energy fluctuations of the OPO/OPA. An absorption cell follows to determine the absorption cross section of a pollutant at a given wavelength.

The main portion of the beam is expanded in a 10:1 telescope to about 2.5-cm diam and transmitted coaxially from the receiving telescope on the roof of our laboratory. This receiving telescope is a 40-cm-diam, $f=3$ Newtonian design. It collects and focuses the backscattered light onto a liquid nitrogen cooled InSb detector.

Figure 2 shows a diagram of the electronics. The amplified signal and reference pulses are integrated and digitized for the computer, which ratios and averages the signals. The signal from the photoacoustic cell is amplified in a lock-in amplifier, which is tuned to the resonance frequency of the cell and synchronized from the trigger signal of the laser.

Wavelength selection of the OPO is controlled by a PDP-11/10 minicomputer. Crystal and grating are set according to values in a table, while the position of the etalon is calculated from a set of parameters. An interactive program was developed to simplify operation of the OPO lidar, and to make automatic measurements possible. Besides service routines for calibration and alignment of the OPO, the program enables automatic scans of the OPO, increasing or decreasing the wavelength in predetermined steps. In another mode the program tunes the OPO between two or three predetermined wavelengths, averages the received signals from each wavelength and also calculates the rms variation of this average for later error analysis. It then calculates the concentration of a pollutant using Eq. (2). This value is displayed in real time as well as stored for later use. This control routine proved to be essential for the measurements reported in later sections of this paper.

Without the etalon in the cavity, the OPO can be scanned under computer control continuously from 1.4 to 4.0 μm, a range of more than 4500 cm^{-1}. Figure 3 shows an example of the scan capabilities of the OPO. In the lower trace it shows an atmospheric transmission spectrum from May 31, 1979. We used a building 775 m away as backscattering target, so the total atmospheric pathlength is 1.55 km. The scan covers a 450-cm^{-1} range from 2850 to 3300 cm^{-1}, which includes numerous absorption lines mainly due to water vapor and methane, although many other trace constituents have absorption lines in this region. To confirm the accuracy of our

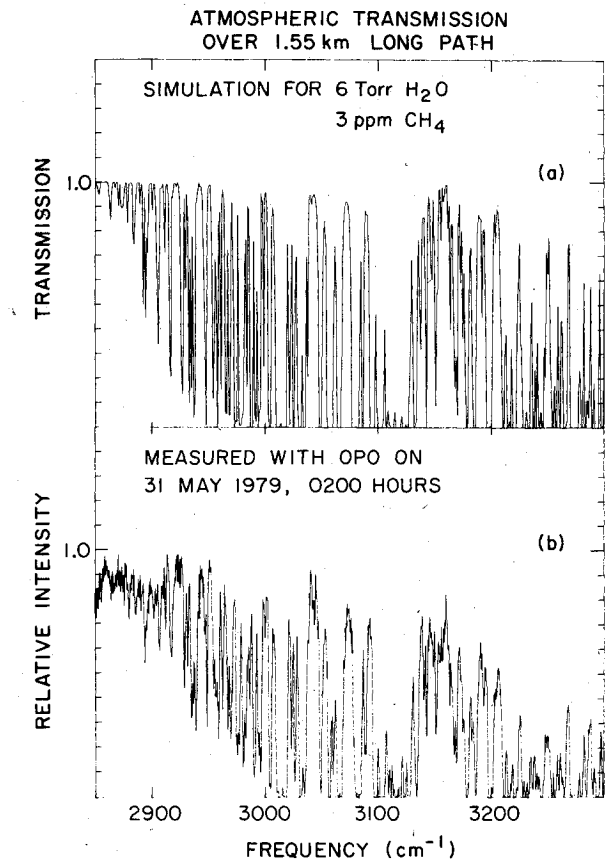

Fig. 3 450 cm^{-1} scan with OPO lidar around 3.0 μm. The lower trace shows the measured transmission, using a building 775 m away as backscattering target. The upper trace shows a simulation of the same transmission spectrum using the AFCRL data base. A linewidth of 1.5 cm^{-1} was assumed for the simulation, but the rectangular lineshape in the simulation does not match well the OPO lineshape.

scan and to identify lines we use the Air Force Cambridge Research Laboratory (AFCRL) data base.[18] The upper trace in Fig. 3 shows a simulated transmission spectrum using the AFCRL data. For this simulation we assumed 6 Torr H_2O and 3 ppm CH_4 in the atmosphere. The linewidth was assumed to be 1.5 cm^{-1}. However, the program that calculates the transmission from the AFCRL data uses a rectangular slit function, which is not a very good approximation of the OPO lineshape, and results in discrepancies between the calculated and the observed spectrum. Nevertheless, the general agreement of both traces in Fig. 3 confirms the usefulness of the OPO source for spectroscopic applications.

It is considerably more complex to control continuous scans with the etalon inserted into the OPO cavity. Grating and etalon position have to be synchronized to within 0.1 cm^{-1}. This requires excellent stability of the tuning mechanism. Furthermore, if a scan over more than one free spectral range of the etalon is required, the etalon has to be reset to its zero position during the scan. The length of a scan is determined by the accuracy with which the etalon free spectral range and the tuning rate of the grating are known. We developed extensive software to measure semiautomatically the etalon parameters and so enable scans over many etalon free spectral ranges. We demonstrated scans over more than 10 free spectral ranges, which in the case of a 2-mm thick fused silica etalon is about 20 cm^{-1}. For our applications, this scan range is more than adequate. Figure 4 demonstrates the scanning capabilities and the linewidth of our OPO source with and without intracavity etalon. It shows the spectrum of the Q-branch of the $2\nu_3$ overtone transition in CH_4 at low pressures obtained in a photoacoustic cell (see also the high resolution

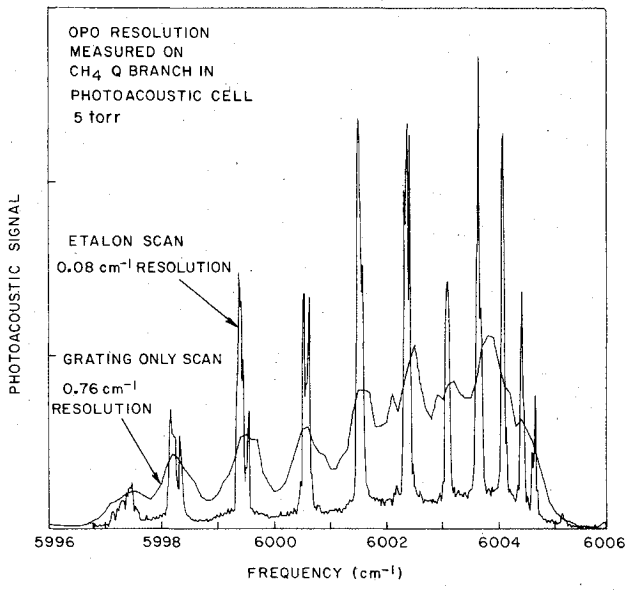

Fig. 4 Photoacoustic spectrum of $2\nu_3$ CH_4 Q-branch at 1.66 μm. The scan is repeated with and without the tilted etalon in the OPO cavity. The linewidth of the OPO in each case is apparent.

spectrum obtained by Bobin[19]). The resolution of the OPO with and without the etalon inserted is apparent. The etalon narrowed the OPO linewidth to 0.08 cm^{-1}.

The reliability of the Nd:Yag OPO transmitter has been demonstrated by more than a year of operation without damage to the pump laser or the OPO. Since the lidar consists only of solid state components, no periodic maintenance is required.

III. Methane Measurements

We selected the measurement of methane concentration to demonstrate the reliability of our system. The atmospheric methane concentration is recorded at the Bay Area Air Quality Management District point monitoring station in Redwood City 10 km from our laboratory. This allows the possibility of comparing the accuracy of our system with an independent station.

Figure 5 shows two transmission spectra near the CH_4 absorption region at 3.4 μm. Both spectra were obtained with the idler output of the OPO/OPA. The linewidth of the output was 1.4 cm^{-1}. The upper trace shows the atmospheric transmission between our system and a building at 775-m distance, which was used as noncooperative backscattering target. Both CH_4 and H_2O absorption lines are present. To clearly identify the CH_4 lines and to aid in selecting a transition that is free of water vapor interference, an absorption spectrum of CH_4 was measured in the laboratory. A section of the scan centered on the P-branch is also shown in the lower trace in Fig. 5. The two scans in this figure can be overlaid to show that the P(2), P(7), P(9), and P(10) methane transitions are nearly water vapor free. Additional confirmation is also obtained from the spectroscopic information in the AFCRL data.[18] The ability to select interference-free absorption bands and to verify the location of spectral lines by scanning the spectrum is a major advantage of the tunable source.

We selected the P(10) transition for our measurements because it has the proper absorption strength for CH_4 measurements over the selected 775-m long path. For measurements over shorter paths, the P(7) line with a much larger cross section can be used. The computer was programmed to tune on and off the P(10) line every 20 pulses or 2 s. The data were normalized and processed to show the concentration of methane. An effective cross section for the CH_4 P(10) line was used based on the resolution of the OPO/OPA source. To correct for any long-term drift, the

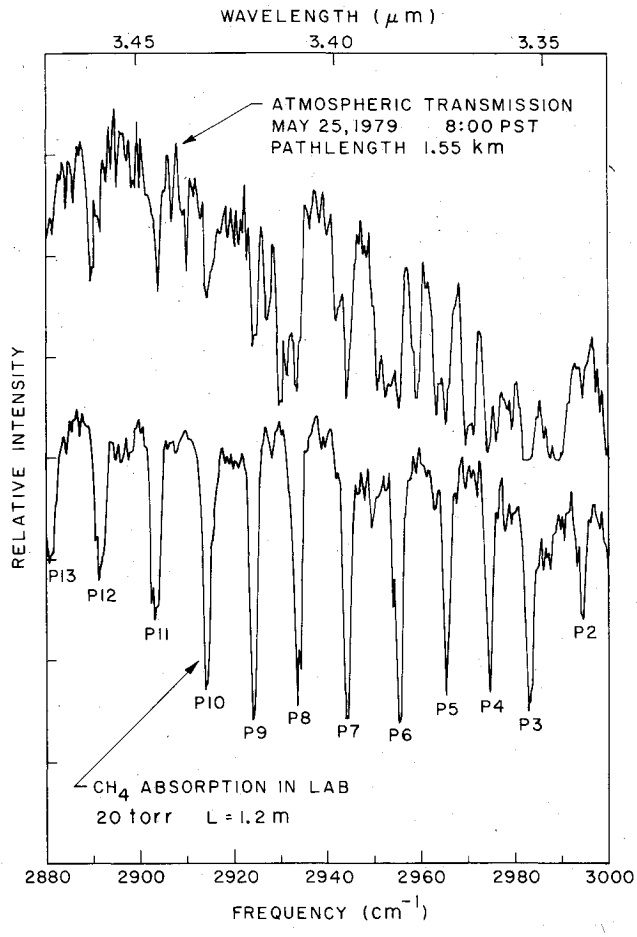

Fig. 5 Transmission spectrum around 3.4 μm. Upper trace shows the atmospheric transmission over a 1.55-km long path. The lower trace is transmission through a 1.2-m long absorption cell filled with CH_4 and N_2 and is used to identify CH_4 lines in the atmospheric spectrum.

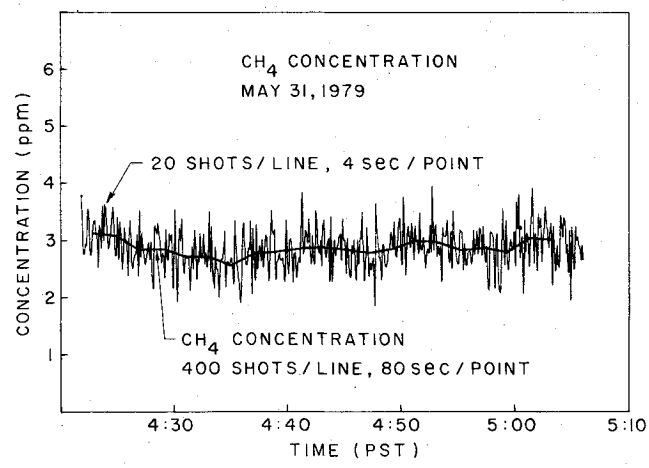

Fig. 6 One hour segment of remote methane measurement, showing CH_4 concentration vs time. Each point represents a 20 shot or 4 s average, and has a rms fluctuation of 0.6 ppm. The heavy line shows same data after later averaging, reducing rms errors to 0.09 ppm.

cross section was measured continuously during a run by the photoacoustic cell. The measured value of the cross section was used to calculate the methane concentration in real time.

Figure 6 shows a segment of a 17-h CH_4 measurement run. Here, the raw measurements are shown for 20 shots/line averaging or 4 s per point. The rms fluctuations are calculated to be 0.6 ppm. To improve the precision of the measurement, longer averaging times can be used. The heavy line in Fig. 6

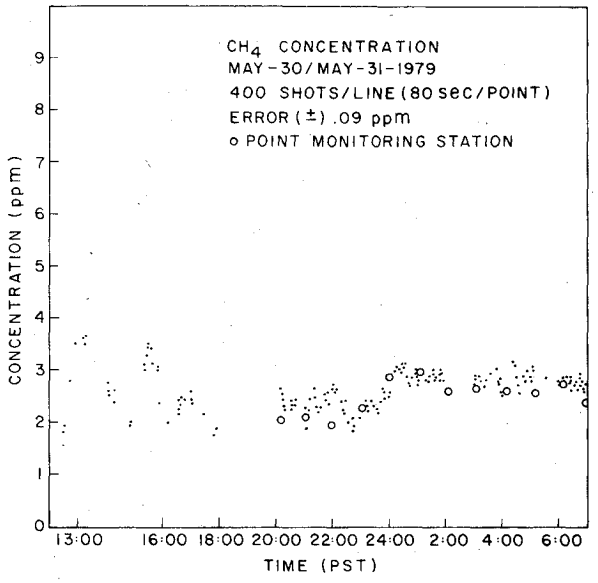

Fig. 7 CH_4 concentration vs time over a 17-h period. Each point is an average over 80 s, reducing rms deviations to 0.09 ppm, which is less than the measured CH_4 fluctuation in the atmosphere. Open circles indicate measured concentrations in Redwood City point monitoring station.

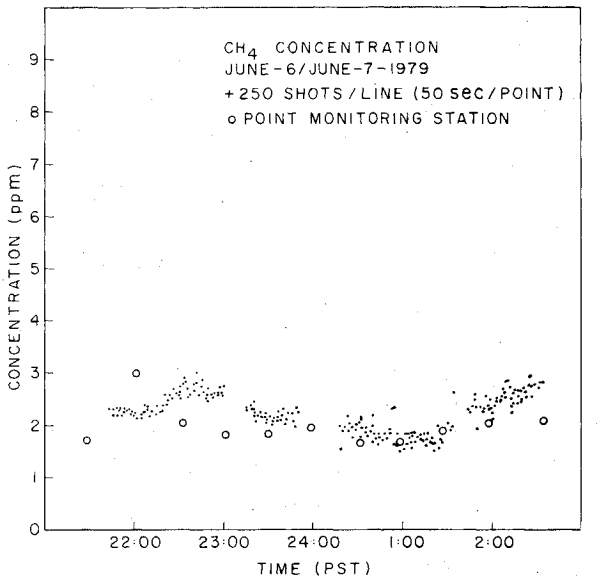

Fig. 8 CH_4 concentration vs time. Stanford lidar data are compared to values from Redwood City point monitoring station 10-km away. Here a prevailing wind yielded a 30 min delay between the atmosphere at point monitoring station and its arrival in Stanford.

shows the same data after later averaging to increase the relative accuracy to 0.09 ppm. The time resolution is 80 s per point in this case.

Figure 7 shows the full 17-h long measurement during which the system was operating automatically under computer control. During the measurements concern developed that the measured CH_4 levels were high since the global average CH_4 level is close to 1.5 ppm. Hourly CH_4 average measurements were obtained from the Redwood City Bay Area Air Quality Management District point monitoring station 10 km from our lidar at Stanford. The concentration measurements from this point monitoring station are indicated by open circles in Fig. 7. The agreement between the concentration values from both measurements is as good as can be expected considering the physical separation between Stanford lidar system and the Redwood City monitoring station.

To check further on the correlation between the Stanford and the Redwood City station measurements, a second extended CH_4 measurement was made on June 6, 1979. Figure 8 shows the results. In this case, the wind was blowing down the bay from Redwood City toward Stanford. The wind velocity and distance gave a 20- to 30-min delay time from Redwood City to Stanford. This delay correlates with the peak CH_4 measurement at 2200 at Redwood City and at Stanford at 2230. Later in the evening when the wind ceased, Stanford measurements became independent of the Redwood City station measurements.

These measurements demonstrate the reliability and accuracy of remote air pollution measurements. Other pollutants with absorption lines within the tuning range of the OPO source can be measured with the same relative accuracy. The measurement of other species is discussed in Sec. V.

IV. Temperature Measurement

For accurate pollutant measurements it is important to determine the temperature of the pollutant, since the absorption cross section is temperature dependent. This effect is usually neglected for the measurement of pollutants at atmospheric temperatures. However for emissions from sources at elevated temperatures the temperature correction can become very important. By properly selecting appropriate lines of a molecular species it is possible to make remote temperature and concentration measurements of the species simultaneously.

A number of groups have proposed and analyzed methods of making remote temperature measurements, and preliminary remote temperature measurements have been reported using Raman lidar[20] and a two-frequency absorption measurement.[21] Remote temperature measurements using atmospheric transmittance measurements of three wavelengths have been analyzed by Mason[22] and Schwemmer and Wilkerson.[23] The temperature dependence of the absorption cross section is given by the Boltzmann distribution and a partition function $Q(T)$ as

$$\sigma(\nu_i,T)=\sigma(\nu_i,T_0)Q(T)\exp\{(E_i^0/k)(1/T_0-1/T)\} \quad (3)$$

for an arbitrary reference temperature T_0, where E_i^0 is the lower state energy of the transition at frequency ν_i, and k is the Boltzmann constant.

Measuring the absorbance

$$A(\nu_i,T)=N\sigma(\nu_i,T)R$$

for two lines of one species with different lower state energy E_i^0 we can use Eq. (3) to determine the temperature T as

$$T=\frac{T_0}{1-\dfrac{kT_0}{E_1^0-E_2^0}\left\{\ln\left(\dfrac{A(\nu_1,T)}{A(\nu_2,T)}\right)-\ln\left(\dfrac{\sigma(\nu_1,T_0)}{\sigma(\nu_2,T_0)}\right)\right\}} \quad (4)$$

This expression simplifies for $T-T_0 \ll T_0$ to

$$T=\frac{kT_0^2}{E_1^0-E_2^0}\ln\left(\frac{A(\nu_1,T)}{A(\nu_2,T)}\right)+D \quad (5)$$

with

$$D=\frac{kT_0^2}{E_1^0-E_2^0}\left\{\ln\left(\frac{\sigma(\nu_2,T_0)}{\sigma(\nu_1,T_0)}\right)\right\}+T_0$$

The constant D can be found either using spectroscopic data, or it can be determined empirically with calibrated temperature measurements. Once the temperature (and so the

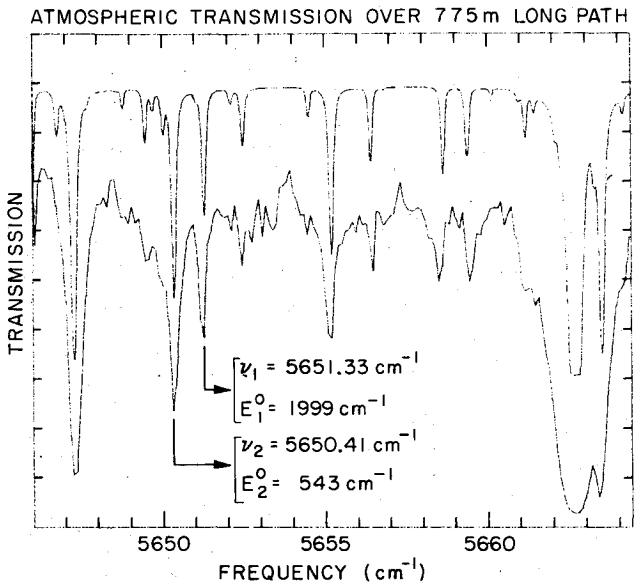

Fig. 9 High resolution atmospheric scan over 1.55-km path. The OPO linewidth is 0.1 cm^{-1}. The OPO transmission scan (lower trace) is compared to a simulation using AFCRL tapes (upper trace).

cross section) is known, it is straightforward to calculate the density of the species using Eq. (2).

The accuracy of a remote temperature measurement is determined by the signal to noise ratio (SNR) and the number of averaged signals (n). From Eq. (5) one finds that

$$\delta T = \left(\frac{kT_0^2}{E_1^0 - E_2^0}\right) \frac{1}{\mathrm{SNR}\sqrt{n}} \left\{\sum_{i=1}^{2} \left(\frac{1+\exp(2A(\nu_i,T))}{A^2(\nu_i,T)}\right)\right\}^{1/2} \quad (6)$$

δT is minimized for $A(\nu_i,T) \simeq 1.1$, where Eq. (6) simplifies to

$$\delta T \simeq 4\left(\frac{kT_0^2}{E_1^0 - E_2^0}\right) \frac{1}{\mathrm{SNR}\sqrt{n}} \quad (7)$$

For an atmospheric temperature measurement, we selected H_2O as absorbing species for the following reasons.

1) H_2O allows simultaneous measurement of temperature and humidity, an important capacity for remote meteorological measurements.

2) Due to the complexity of the H_2O spectrum, nearby lines with a large lower state energy difference can be found. This simplifies the measurement since the transmitter has to be tuned only over small wavelength increments.

3) Lines generating the appropriate absorbance to minimize Eq. (6) for different pathlengths can be found.

We used the AFCRL-tapes[18] to select appropriate H_2O lines for temperature and humidity measurements over a 755-m long path (for a discussion of this line selection see Ref. 24). We selected two lines of the 1.9-μm H_2O band at 5650.41 cm^{-1} and 5651.33 cm^{-1}. The difference in lower state energy is 1456 cm^{-1}. From Eq. (7), we estimate a temperature accuracy of 1°C for a product of $\mathrm{SNR}\sqrt{n} = 175$. For a SNR of 25, this means a 50 shot average, which promises a good time resolution for this measurement.

The lower trace in Fig. 9 shows an atmospheric transmission scan with a 0.1-cm^{-1} resolution tuned over a 17-cm^{-1} range around the selected lines. The upper trace is a simulated transmission spectrum, using AFCRL-tapes.[18] We used scans similar to this to calibrate the tuning of the OPO and to identify the temperature sensitive lines.

Once the wavelength of these lines is determined and the OPO aligned, measurements of temperature and humidity are done under computer control. The return signal at each

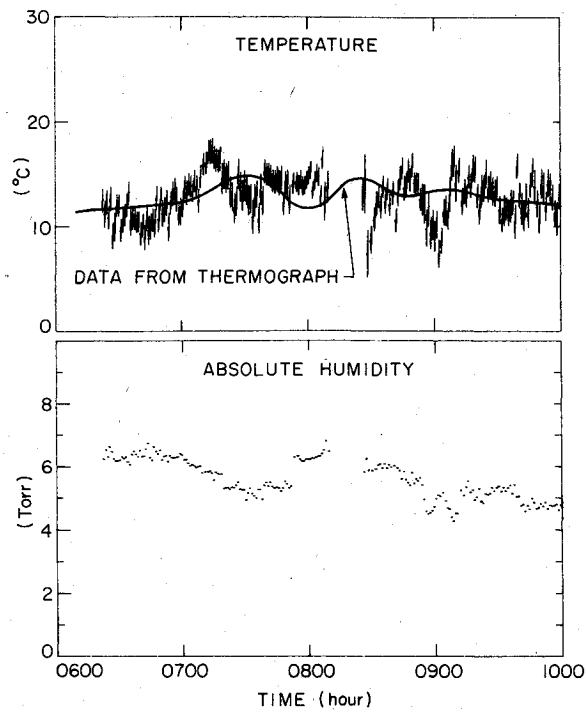

Fig. 10 Temperature and absolute humidity measurement from the morning of March 11, 1980. Temperature data are compared with records from thermograph at receiving telescope.

frequency is averaged over several shots before tuning to another wavelength. To keep errors due to water vapor fluctuations small, it is desirable to tune the OPO after each shot and average the temperature data afterward. However, tuning between different wavelengths takes up to 0.5 s. To improve the time resolution of our measurements we average 30 shots per line before tuning to the next line. When all three required wavelengths are probed, temperature and humidity are calculated. This cycle continues, until a total number of 150 shots per line is reached. Then the computer calculates the average of five temperature and humidity data points as well as the error due to return signal fluctuations, stores, and displays those values.

Figure 10 shows the record of temperature and humidity from the morning of March 11, 1980. Each point represents an average of 150 shots/line, or a time resolution of 45 s. The outside weather was cloudy at first, with rain starting at 0740. The rain increased until it was so strong at 0810 that the measurement had to be interrupted. At 0820 the rain stopped, the cloud cover slowly dissipated, and the wind increased. The remotely measured temperature is compared with a record of a thermograph at the telescope. The general agreement is good. Some discrepancies of the two measurements are expected since the remote measurement averages over a path from 10 to 60 m above the ground and 775-m length, while the thermograph is located on the roof of a building. The rms deviation for each temperature measurement is calculated from the return signal fluctuations. It varies with the meteorological conditions: in the early morning, the SNR was measured to be 25. The variance of the temperature measurements then is 1.1°C, which is only slightly worse than the estimate in Eq. (7). The SNR decreases later due to the rain, and accordingly the rms-deviations increase to 1.6°C. After the rain stopped, the SNR improved again to about 25. However, the temperature uncertainty stays at 1.5°C. The reason for this increased error can be found in the stronger humidity fluctuations due to the wind. Any variation in absolute humidity during the 10 s measurement cycle for each temperature point increases the uncertainty of this measurement. Shorter measurement cycles will improve the accuracy of the measurement.

Table 2 Predicted measurement capabilities for the OPO lidar

Species	Absorption cross section, [atm cm]$^{-1}$	At wavelength, [cm]$^{-1}$	Predicted sensitivity, ppm km	Atmospheric concentrations
CO_2	0.02	4969	2.5	Background 330 ppm
CO	0.3	4285	0.3	In pollution 30-50 ppm
SO_2	0.4	2499	0.25	In sulfurous smog 1 ppm
NO_2	3.2	2913-2928	0.03	In photochemical smog 0.1 ppm
N_2O	2.3	2578	0.05	Background 0.29 ppm
HCHO	$\simeq 10$	2898	0.01	In photochemical smog 0.05 ppm
HCl	$\simeq 10$	2822-2955	0.01	1-5 ppm locally
CH_4	>40	3030-2910	0.005	1.5 ppm background
Ethane	13	2976.8	0.010	Concentration of
Ethylene	1.7	2962.5	0.060	all hydrocarbons except CH_4
Propane	>50	2967.6	0.010	<0.25 ppm in 3-h average
H_2O	wide range selectable		1%	1-2%
Temperature using H_2O	0.005	5650,5651	1°C	

The calibration of our temperature data is done by minimizing the difference between the remote temperature data and the thermograph data. We have collected more than 10 h of temperature data, and have determined a value for the constant D as 35°C, which is 19°C less than predicted from the available spectroscopic data.

We have demonstrated the feasibility to measure temperature and humidity simultaneously. The 1.9-μm H_2O band makes temperature measurements with 1.0°C accuracy possible. For the present measurements of atmospheric temperature the selected lines are optimal. However, for temperature measurements at elevated temperatures, such as encountered in stack exhausts, a different selection of lines has to be made.

V. Measurement of Other Atmospheric Trace Constituents

In this section we discuss the possibility of measuring other trace constituents in the atmosphere with the OPO lidar. Most pollutants have absorption bands in the 1.4 to 4.0-μm tuning range of the OPO. However, some of the lines are too weak to measure atmospheric concentrations, while others lie in regions of strong water vapor absorption, which makes measurements over long paths impossible.

To estimate the sensitivity of a measurement of a certain species it is assumed that a 1% change in transmission can be measured. For the reported measurements this is true for averages between 150 laser pulses per line for the H_2O measurements, to 2000 pulses per line for the CH_4 measurements, which means averaging times between 30 and 400 s. The variation of the averaging time is due to the variation of the output energy and pulse to pulse stability of the OPO over its tuning range, but also due to water vapor continuum absorption around 3.4 μm (Ref. 18).

Measurement capabilities of the major pollutants as identified by Wright et al. in Ref. 25 is now discussed. Spectroscopic information was obtained from different sources, the AFCRL data base[18] being the most important one since it contains the major atmospheric constituents and is ideally suited to check for interferences of different species. An overview over the measurement capabilities is summarized in Table 2.

H_2O

The influence of water vapor on atmospheric processes and measurements is so important that it must be discussed first. The measurement of humidity easily is possible in the infrared, as was demonstrated in Sec. IV. A large number of lines exist, which makes it possible to select one with the ideal cross section for a specific measurement. The two water vapor absorption bands of importance for measurements with the OPO transmitter are the 1.9- and 2.7-μm bands. These bands absorb so strongly that measurements over long paths in the regions from 1.8 to 2.0 μm and 2.4 to 3.2 μm are not possible. The surrounding regions contain lines of ideal strengths for atmospheric humidity measurements. The large number of water vapor lines leads to interference problems in the measurements of many other pollutants. Thus it is necessary to measure the absolute humidity first in order to correct absorption measurements on pollutant lines influenced by nearby H_2O lines.

CO_2

On a global scale, carbon dioxide is important to monitor due to its effect on the thermal balance of the atmosphere.[26] On a local scale, CO_2 can be used as a tracer for emissions from combustion processes, and to measure the temperature of these emissions. The atmospheric background of CO_2 is 330 ppm in an unpolluted atmosphere, and ranges up to 350 ppm in polluted regions. For remote measurements with the OPO transmitter, the $\nu_1+2\nu_2+\nu_3$ combination band at 4983 cm^{-1} is ideal. Using the AFCRL data base[18] and our own atmospheric transmission spectra we determined that the P(8), P(10), and P(36) lines are interference free from water vapor absorption. These lines are well suited to measure atmospheric background as well as source emissions of CO_2. Using the 570-cm^{-1} lower level energy difference of the P(8) and the P(36) lines, temperature of sources can be determined with a 5°C accuracy.

CO

Carbon monoxide is known to be a health hazard in high concentrations. The Clean Air Act sets the CO exposure limit to an average value of less than 35 ppm over 1 h or 9 ppm over 24 h. Remote monitoring simplifies the task of measuring ambient concentrations and emissions. Measurements of CO with the OPO is possible at the overtone band at 4260 cm^{-1} (Ref. 27). Many lines without water vapor interference can be found. The absorption cross section is approximately 0.4 [atm cm]$^{-1}$ (Ref. 18) which leads to a measurement sensitivity of 0.3 ppm km. The measurement of atmospheric background concentrations of CO in unpolluted atmospheres is difficult, but the observation of pollution and measurements of source emissions are possible.

SO_2

Sulfur dioxide is the major pollutant in sulfurous smog. It has been recognized as a health hazard, and the Clean Air Act requires annual average SO_2 concentrations of less than 0.03 ppm, although over a 3 h period the average may be as high as 0.50 ppm. We have demonstrated the possibility of measuring sulfur dioxide with the OPO lidar earlier.[12] The $\nu_1+\nu_3$

combination band around 2499 cm^{-1} has linestrengths of 0.4 [atm cm] $^{-1}$ (Ref. 28), which makes measurements of concentrations of 0.25 ppm km possible. However, this measurement has to be made near the end of the tuning range of the $LiNbO_3$ OPO, where the energy output is low and pulse energy fluctuations are increased. Thus a large number of laser pulses have to be averaged to achieve the desired sensitivity. However, measurements of source emissions and monitoring of SO_2 polluted atmospheres is possible.

O_3

Ozone is a major constituent in photochemical smog. There is a natural ozone background of 0.01 ppm, but its concentration reaches 0.3 ppm in photochemical smog.[25] Within the tuning range of the OPO, the strongest absorption band is the $3\nu_3$ band at 3050 cm^{-1}. The strongest lines are about 0.3 [atm cm] $^{-1}$ (Ref. 18), which leads to a sensitivity of 0.3 ppm km. This value is not adequate to measure atmospheric ozone with the OPO lidar.

NO_x

Nitrogen oxides are important in photochemical smog. Their primary anthropogenic source is combustion. In polluted urban regions the concentration of NO_2 may be 0.1 ppm, or even higher in exceptional circumstances. The measurement of NO is not possible with the OPO lidar, since only a weak overtone transition exists at 4746 cm^{-1}; but NO_2 has relatively strong lines in the $\nu_1+\nu_3$ band at 2910 cm^{-1}. From spectra in Ref. 29, the strongest line has a strength of 3.2 [atm cm] $^{-1}$, which allows measurements with a 0.03 ppm km sensitivity. Measurements of sources as well as monitoring of polluted regions is possible. However, potential interference from water and hydrocarbon lines makes careful line selection necessary to minimize interference with those species.

N_2O

Another nitrogen compound in the atmosphere is nitrous oxide. There is an atmospheric N_2O concentration of 0.29 ppm, which is caused mainly by biological action in soil. It is inert in the troposphere but of interest due to its interaction with ozone in the stratosphere.[30] The absorption band at 2545 cm^{-1} is strong enough to promise a sensitivity of 0.05 ppm km, and interference free lines can be found.[18] This allows measurements of atmospheric background concentrations of nitrous oxide.

NH_3

Another pollutant of importance is ammonia. Its strongest absorption bands within the tuning range of the OPO are around 3400 cm^{-1} (Ref. 31). However, we have not found spectra of adequate accuracy to determine if absorption measurements are possible using lines located in the strong surrounding water vapor absorption region.

HCHO

Formaldehyde also is a component of photochemical smog. Its atmospheric concentration varies between 1 and 50 ppb.[25] The cross sections of lines around 2800 cm^{-1} from Ref. 29 promise a sensitivity of 0.01 ppm km, which makes long path measurements suitable to monitor formaldehyde concentrations in smog conditions.

HCl

The natural background of hydrogen chloride is negligibly small, but anthropogenic sources can release HCl in large quantities that lead to concentrations of 1-5 ppm (Ref. 25). HCl has very strong absorption lines around 2900 cm^{-1}. From the spectrum in Ref. 29 we determine cross sections of 10 [atm cm] $^{-1}$, which allows sensitivities of 0.01 ppm km. Since several lines can be selected, interference from water vapor and hydrocarbons can be minimized. Measurements of HCl are possible with the OPO lidar.

Hydrocarbons

Hydrocarbons are important in photochemical processes. Only methane has a large background in unpolluted atmospheres, all other hydrocarbons arise mainly from anthropogenic sources.[25] The major sources are combustion and chemical processes. All hydrocarbons have a very strong ν_3 vibration band, but interferences with water vapor lines as well as other hydrocarbons cause problems for the measurements of some of them. Methane has a background concentration in an unpolluted atmosphere of 1.5 ppm. We have discussed the measurement of CH_4 with the OPO lidar in Sec. III and demonstrated the sensitivity in such a measurement.

The other hydrocarbon components play a more important role in photochemical smog than methane. However, due to the difficulties in measuring them independently, little is known about reactions of specific components in the atmosphere. With the OPO lidar a large number of hydrocarbons can be measured with good sensitivity. However, water vapor, methane, and other components all have to be measured simultaneously due to interference of lines. Using high resolution spectra obtained with the EPA ROSE System,[32] we identified measurement possibilities for ethane, propane, and ethylene.

Ethane can be measured at 2976.8 cm^{-1}, where it has an absorption line with a strength of 13 [atm cm] $^{-1}$. This line is overlapped by a water vapor line, but transmission on this wavelength is adequate for the use of long paths. This line promises a sensitivity of 8 ppb km, if errors due to the measurement of H_2O concentration can be neglected.

Propane has a very strong line at 2967.6 cm^{-1}, the absorption cross section was determined as 83 [atm cm] $^{-1}$. However, H_2O, CH_4, and other hydrocarbons have absorption lines close to this wavelength, and their interference reduces the sensitivity. Nonetheless, a 10 ppb km sensitivity still can be expected.

Ethylene has a relatively strong line at 2980 cm^{-1}, but this line is completely obscured by a strong water vapor line. Measurement is possible at 2962.5 cm^{-1}, but line strength here is only 1.7 [atm cm] $^{-1}$, which does not promise the measurement of traces in the atmosphere. Other hydrocarbon components have to be evaluated in detail.

VI. Conclusions

We demonstrated the capabilities of a $LiNbO_3$ OPO as a lidar transmitter. The OPO has a tuning range of 4500 cm^{-1} from 1.4 to 4.0 μm. The linewidth is less than 1 cm^{-1}, and can be reduced to 0.1 cm^{-1} by insertion of a tilted etalon. Wavelength selection of the OPO is done under computer control. An extensive software routine was developed to control automatic measurements.

Reliability of the system was demonstrated in a series of remote methane measurements at 3.4 μm over a 775-m long atmospheric path, using a building as noncooperative backscattering target. The longest of these measurements was over a period of 18 h, during which the system operated automatically under computer control. Our concentration measurements were compared with those of a nearby point monitoring station. The agreement was excellent.

The advantages of a continuously tunable infrared transmitter were further demonstrated with a measurement of meteorological importance. We measured simultaneously average temperature and humidity over the 775-m long path. We selected for this measurement two nearby lines in the 1.9-μm water band, which have a 1456 cm^{-1} lower level energy difference and so promise a good temperature sensitivity and are of similar strength. Using those lines, we measured temperature with a 1°C relative error, while humidity data have a relative error of 1%.

In addition to the described measurements, a large number of other trace constituents can be measured. We used available spectroscopic data to identify the sensitivity for

measurements of the most important trace constituents in the troposphere. We found, that background concentrations of some pollutants can be measured. Source emission monitoring is feasible for most important pollutants with the OPO lidar.

The transmitter source can be improved. An increase of output energy to more than 70 mJ is possible. With this amount of transmitted energy, depth resolved measurements using Mie scattering as a distributed reflector are possible. This will have advantages for source monitoring applications. For the measurement of ambient background concentrations, however, a monostatic system like the one described here promises the highest sensitivity.

Acknowledgments

We want to acknowledge helpful discussions with Dr. E. R. Murray of S.R.I. International and Dr. W. F. Herget of the Environmental Protection Agency. We also would like to acknowledge the loan of the receiving telescope by the Electric Power Research Institute and support for this program by the Army Research Office under Contract DAAG29-77-G-0181.

References

[1] Hinkley, E. D., *Remote Probing of the Atmosphere,* Springer Verlag, Berlin, 1976.

[2] Kildal, H. and Byer, R. L., "Comparison of Laser Methods for Remote Detection of Atmospheric Pollutants," *Proceedings of the IEEE,* Vol. 59, 1971, p. 1633.

[3] Byer, R. L. and Garbuny, M., "Pollutant Detection by Absorption Using Mie Scattering and Topographic Targets as Retroreflectors," *Applied Optics,* Vol. 12, 1973, p. 1496.

[4] Byer, R. L. and Murray, E. R., "Remote Monitoring Techniques," *Handbook of Air Pollution Analysis,* edited by R. Perry and R. Young, Chapman Hall, London, 1977.

[5] Rothe, K. W., Brinkmann, U., and Walther, H., "Applications of Tunable Dye Lasers to Air Pollution Detection: Measurement of Atmospheric NO_2 Concentrations by Differential Absorption," *Applied Physics,* Vol. 3, 1974, p. 115.

[6] Grant, W. B., Hake, R. D., Liston, E. M., Robbins, R. C., and Proctor, E. K., "Calibrated Remote Measurement of NO_2 Using the Differential Absorption Backscatter Technique," *Applied Physics Letters,* Vol. 24, 1974, p. 550.

[7] Frederikson, K., Galle, B., Nystrom, K., and Svanberg, S., "A Mobile LIDAR System for Measurements of NO_2, SO_2, O_3, and Particles," IX International Laser Radar Conference, Munich, Germany, 1979.

[8] Hawley, J. G., Fletcher, L. D., Wallace, G. F., and Herron, M., "A Mobile Differential Absorption Lidar (DIAL) for Range Resolved Measurements of SO_2, O_3, and NO_2," X International Laser Radar Conference, Univ. of Maryland, 1980.

[9] Baumer, W., Rothe, K. W., and Walter, H., "Range Resolved Measurements of Atmospheric Pollutants," IX International Laser Radar Conference, Munich, Germany, 1979.

[10] Killinger, D. K., Meynuk, N., and DeFeo, W. E., "Remote Sensing of CO Using Frequency Doubled CO_2 Laser Radiation," *Applied Physics Letters,* Vol. 36, 1980, p. 402.

[11] Altmann, J., Lahmann, W., and Weitkamp, C., "Remote Measurements of Atmospheric N_2O with a DF Laser Lidar," *Applied Optics,* Vol. 19, 1980, pp. 34-53.

[12] Baumgartner, R. A. and Byer, R. L., "Remote SO_2 Measurements at 4 μm with a Continuously Tunable Source," *Optics Letters,* Vol. 2, 1978, p. 163.

[13] Baumgartner, R. A. and Byer, R. L., "Continuously Tunable IR Lidar with Applications to Remote Measurements of SO_2 and CH_4," *Applied Optics,* Vol. 17, 1978, p. 3555.

[14] Brosnan, S. J. and Byer, R. L., "Optical Parametric Oscillator Threshold and Linewidth Studies," *IEEE Journal of Quantum Electronics,* Vol. QE-15, 1979, p. 415.

[15] Baumgartner, R. A. and Byer, R. L., "Optical Parametric Amplifiers," *IEEE Journal of Quantum Electronics,* Vol. QE-15, 1979, p. 432.

[16] Endemann, M. and Byer, R. L., "Remote Probing of Atmospheric Methane over Long Timescales Using a Widely Tunable Source," Post Deadline Paper, IX International Laser Radar Conference, Munich, West Germany, 1979.

[17] Klauminzer, G. K., "New High Performance Short Cavity Dye Laser Design," Post Deadline Paper, Conference on Laser Engineering and Applications, Washington, D. C., 1977.

[18] McClatchey, R. A. et al., "AFCRL Atmospheric Absorption Line Parameter Compilation," AFCRL Rept. TR-73-0096, 1973.

[19] Bobin, B., "Interpretation de la Bande Harmonique $2\nu_3$ du Methane $^{12}CH_4$ (De 5890 a 6107 cm^{-1})," *Journal de Physique,* Vol. 33, 1972, p. 345.

[20] Cohen, A., Cooney, J. S., and Gelleo, K. N., "Atmospheric Temperature Profiles from LIDAR Measurements of Rotational Raman and Elastic Scattering," *Applied Optics,* Vol. 15, 1979, p. 2896; see also, Gill, R., Geller, K., Farina, J., Cooney, J., and Cohen, A., *Journal of Applied Met.,* Vol. 18, 1979, p. 225.

[21] Murray, E. R., Powell, D. D., and van der Laan, J. E., "Measurement of Average Atmospheric Temperature Using CO_2 Laser Radar," *Applied Optics,* Vol. 18, June 1980.

[22] Mason, J. B., "Lidar Measurement of Temperature: A New Approach," *Applied Optics,* Vol. 14, 1975, p. 76.

[23] Schwemmer, G. K. and Wilderson, T. D., "LIDAR Temperature Profiling: Performance Simulations of Mason's Method," *Applied Optics,* Vol. 18, 1979, p. 3539.

[24] Endemann, M. and Byer, R. L., "Remote Single Ended Measurements of Atmospheric Temperature and Humidity at 1.9 μm Using a Continuously Tunable Source," *Optics Letters,* Vol. 5, 1980, p. 452.

[25] Wright, M. L., Proctor, E. K., Gasiorek, L. S., and Liston, E. M., "A Preliminary Study of Air Pollution Measurements by Active Remote Sensing Techniques," NASA CR-132, 1975, p. 724.

[26] Moeller, F., "On the Influence of Changes in the CO_2 Concentration in Air on the Radiation Balance of the Earth's Surface and on the Climate," *Journal of Geophysical Research,* Vol. 68, 1963, p. 3877.

[27] Henningson, T., Garbuny, M., and Byer, R. L., "Remote Detection of CO by Parametric Tunable Laser," *Applied Physics Letters,* Vol. 24, 1974, p. 242.

[28] Pine, A. S. and Moulton, P. F., "Doppler Limited and Atmospheric Spectra of the 4 μm $\nu_1+\nu_3$ Combination Band of SO_2," *Journal of Molecular Spectrometry,* Vol. 64, 1977, p. 15.

[29] Hanst, P. L., "Spectroscopic Methods for Air Pollution Measurements," *Advances in Environmental Science and Technology,* Vol. 2, edited by J. N. Pitts Jr. and R. L. Metcalf, Wiley Interscience, New York.

[30] Hutchinson, G. L. and Morier, A. R., "Nitrous Oxide Emissions from an Irrigated Cornfield," *Science,* Vol. 205, 1979, p. 1125.

[31] Herzberg, G., *Molecular Spectra and Molecular Structure: II. Infrared and Raman Spectra of Polyatomic Molecules,* D. van Nostrand Company, Inc., 1943.

[32] Herget, W. F., private communication, Nov. 1980.